 doi:10.20944/preprints202106.0503.v1

Article

Hydrological connectivity in a permafrost tundra landscape near Vorkuta, North-European Arctic Russia

Nikita Tananaev [1,*], Vladislav Isaev [2], Dmitry Sergeev [3], Pavel Kotov [2] and Oleg Komarov [2]

[1] P.I. Melnikov Permafrost Institute, Siberian Branch, Russian Academy of Sciences; TananaevNI@mpi.ysn.ru
[2] Lomonosov Moscow State University; tpomed@yandex.ru
[3] Sergeev Institute of Environmental Geoscience; serguuevdo@mail.ru
* Correspondence: TananaevNI@mpi.ysn.ru

Abstract: Hydrochemical and geophysical data collected during a hydrological survey in September 2017, reveal patterns of small-scale hydrological connectivity in a small water track catchment, north-European Arctic. Elevated tundra patches underlain by sands were disconnected from the stream and stored precipitation water from previous months. At the catchment surface and in the water track thalweg, some circular hollows, from 0.2 to 0.4 m in diameter, acted as evaporative basins with low *d*-excess values, from 2 to 4‰. Other hollows were connected to shallow subsurface runoff, yielding *d*-excess values between 12 and 14‰. 'Connected' hollows yielded a 50% higher dissolved organic carbon (DOC) content, 17.5±5.3 mg/L, than the 'disconnected hollows, 11.8±1.7 mg/L. Permafrost distribution across the landscape is continuous, but highly variable. Open taliks exist under fens and small hummocky depressions, as revealed by electric resistivity tomography surveys. Isotopic evidence supports upward subpermafrost groundwater migration through open taliks under water tracks and fens/bogs/depressions, and its supply to streams via shallow subsurface compartment. Temporal variability of isotopic composition and DOC in water track and a major river system, the Vorkuta R., evidence the widespread occurrence of the described processes in the large river basin. Water tracks effectively drain the tundra terrain and maintain xeric vegetation over the elevated inter-track tundra patches.

Keywords: permafrost hydrology; Russian Arctic; water tracks; hydrological connectivity; stable water isotopes; dissolved organic carbon; electrical resistivity tomography; taliks

1. Introduction

Hydrologic connectivity is a complex concept referring to water transfer in the landscape, or between landscapes, or, more generally, within or between the water cycle units, and its (dis)continuity along the major water transport pathways acting on the watershed [1-3]. Connectivity exists between larger domains, *e.g.*, surface runoff and groundwater flow, landscape elements and fluxes – *structural connectivity*, and between processes – *functional connectivity* [4,5].

Permafrost significantly alters the water cycling through the affected landscapes compared to temperate catchments [6-8]. In continuous permafrost, water transport is mostly confined to the active layer and driven by processes related to phase transition in soils [9,10], the reservoir structure is simplified and existing connections between compartments are exposed [11,12]. Open talik zones are frequently detected under largest lakes using geophysical methods [13-15], and may serve as pathways for both upward and downward water migration, connecting surface water to intra- and subpermafrost aquifers [16,17]. In discontinuous permafrost, with deeper active layer, appearance of residual thaw layers, permafrost fragmentation and abundance of talik zones, the potential of water exchange between the compartments is significantly higher [18-20].

Water stable isotopes are widely used to track water sources and hydrologic connectivity across the compartments and ecosystem classes, including boreal and perma-

Preprints (www.preprints.org) | NOT PEER-REVIEWED | Posted: 21 June 2021 doi:10.20944/preprints202106.0503.v1

frost-affected catchments [21-24]. Isotopic evaporation signal allows tracing connectivity between wetlands and perennial streams and modeling surficial wetland runoff contribution to streams during summer [25]. Isotope mass balance reveals the specifics of the permafrost thaw cycle in continuous permafrost [26,27] and is successfully applied to contemporary lakes and lacustrine paleoenvironments [28].

In discontinuous permafrost, taliks of different kinds, including residual thaw layers, are responsible for conveying water from the slopes toward the streams [29,30]. In the Northern Yenisey region, evaporated water sources from late summer precipitation and thermokarst lakes were found to contribute significantly to the winter runoff through the residual thaw layer, an interface between the seasonally freezing layer and the top of permafrost [31]. In the Ob R. basin, strong evaporation signal persists in most river samples in late autumn and around spring freshet dates, evidencing subsurface connections between lakes and rivers of the region [32]. Lake-to-river connectivity is also maintained through sub-lacustrine taliks, both open and closed, developing even under shallow thermokarst lakes [33]. Geophysical techniques, notably electrical resistivity tomography, are useful in describing the complex frozen ground configuration in discontinuous permafrost [34,35].

The climate change presently occurring in the Arctic, followed by the deepening of the active layer, may lead both to the rebuilding connectivity patterns and to an increase in groundwater discharge in hillslopes [36], affecting future dissolved organic carbon and other constituent fluxes [37]. Trends in regional climate and hydrology may also imply changes in fluvial activity [38], though the latter is showing only minor signs in the first-order fluvial network of the region.

This study was conceived to better understand the water and dissolved organic material transport in discontinuous permafrost environment at a small scale. We present new data on water stable isotope composition and dissolved organic carbon (DOC) concentrations from several Subarctic streams and water bodies in minor tundra water track catchments near Vorkuta, north-European Russia. These data are used to trace water origin in these water objects under late summer conditions, around maximum thaw period, and evaluate micro-scale hydrologic connectivity in the landscape. Geophysical survey data are used to support the discussion on surface water interaction with groundwater. The study region, with its mild and humid Subarctic climate, may serve a model region for other permafrost regions in transition under observed climate change.

2. Study area

Fieldwork was performed in September 2017 in north-European Russia, on the margin of the Bolshaya Zemlya tundra region, about 30 km to the south-west from Vorkuta, Komi Republic (Figure 1a). Major sampling effort was concentrated around Khanovey, an abandoned settlement for railroad workers on the right bank of the Vorkuta R., where seasonal permafrost research station is maintained by the Department of Geocryology, Moscow State University (Figure 1b) [39]. The studied location occupies a typical periglacial landscape at the southern margin of the Bolshaya Zemlya tundra, hilly with gently rolling slopes dissected by hummocky depressions and first-order stream valleys. Permian bedrock, exposed locally in the Vorkuta R. bluffs, is overlaid with Quaternary deposits, mostly loams and loamy clays, with variable ice content [39].

Meso-scale topography is dominated by smoothed hilly chains, or *uvals*, with submeridional orientation and elevation between 170 and 200 m a.s.l., divided by the valleys of the Usa R. and its major right tributaries, the Vorkuta R. and Seida R. The *uvals* surface is an undulating plain, hosting numerous lakes, peatlands, and a network of overwetted depressions, locally with mires, presumably of thermokarst origin. On the slopes descending toward the major rivers this network evolves from chaotic to linearly-shaped fluvial network hosting intermittent streams (Figure 2), again becoming poorly organized toward the foot slope, with overwide valleys resembling those of organic-rich and wide water track classes [40].

Preprints (www.preprints.org) | NOT PEER-REVIEWED | Posted: 21 June 2021 doi:10.20944/preprints202106.0503.v1

Interfluves are scarcely vegetated because of blowing snow removal and lower soil temperatures, and lichens are omnipresent. Locally, moss-dominated mires with *Sphagnum sp* occur in topographical depressions in the interfluve belt. Gentle slopes are covered by creeping willow (*S. arctica*), dwarf birch (*B. nana*) and Labrador tea (*L. palustre*), small deciduous shrubs (blueberry, blackberry and cowberry). Water track valleys are willow-dominated, mainly *S. phylicifolia*, with *Equisetum arvensis* and *Carex* spp.

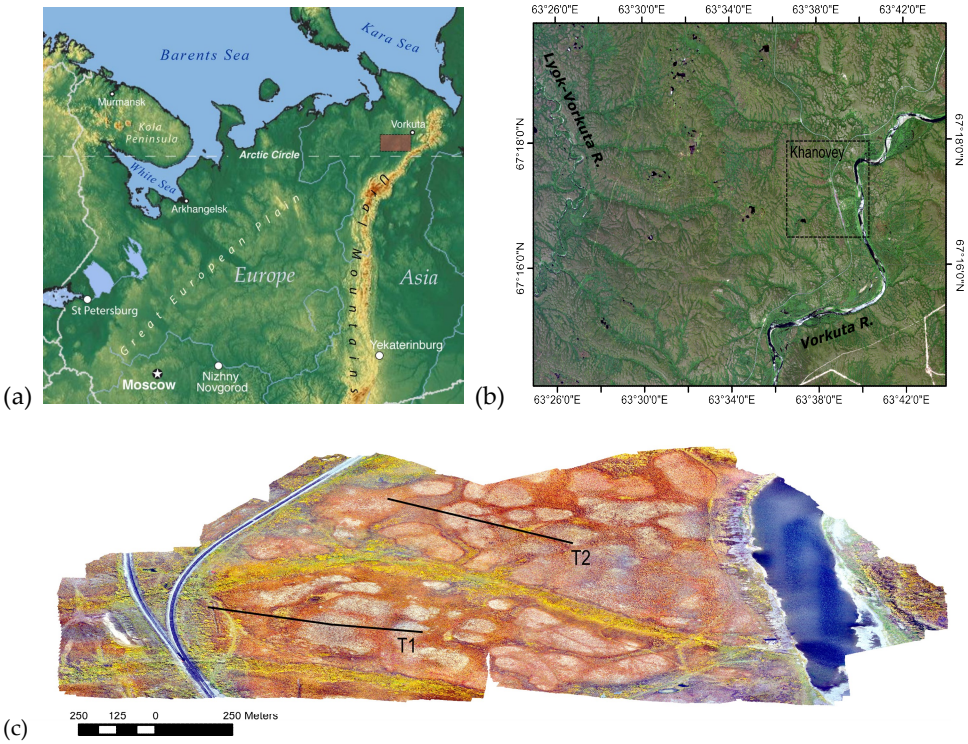

Figure 1. Geographical location of the study site, (a) in north-European Russia, (b) at the Vorkuta R. valley slope; (c) reference orthophotoimage of the studied water track section, T1 and T2 denote the ERT profiles.

Figure 2. Typical midslope landscape of the study region, with minor (first-order) water tracks on the background, a second-order water track feature crossing the image left to right, all easily detectable by its contrasting foliage colour, and elevated tundra patches and intertracks with *B. nana* and lichen patches.

The studied territory occupies the interfluve area between the Vorkuta R. and its right tributary, the Lyok-Vorkuta R., and the valley slope inclined toward the east, to the

Preprints (www.preprints.org) | NOT PEER-REVIEWED | Posted: 21 June 2021 doi:10.20944/preprints202106.0503.v1

Vorkuta R. valley (Figure 1b). This slope is dissected by three first-order water track valleys, one of which was studied in detail in its middle and lower reach, below the railroad crossing (Figure 1c). The water track valley is oriented west-to-east. Its headwaters are connected, via a network of wet depressions and mires, to the headwaters of all major neighboring water tracks, so that no interfluve exist between the water track systems draining in different directions. The basin area of the studied water track, for this particular reason, is estimated around 0.901 km^2 with significant uncertainty.

Regional climate is Subarctic, summer is short and cool, and winter is long and cold, lasting over eight months from October to May (Table 1). At the same time, the period without negative daily temperatures is only 70 days in average year. Mean annual daily temperature is -5.6°C. Precipitation is *ca.* 430 mm, of which from 50 to 70% fall as snow, which can occur at any month of the year.

Table 1. Mean monthly air temperature T, °C and precipitation P, mm, observed at Vorkuta meteo station (1927-2019).

	Jan	Feb	Mar	Apr	May	Jun	Jul	Aug	Sep	Oct	Nov	Dec
T	-19.9	-19.7	-15.4	-9.3	-2.2	7.1	12.7	9.7	4.2	-4.2	-12.9	-17.0
P	22	18	20	24	32	48	59	59	54	40	30	25

Permafrost is continuous, with thickness varying from 50 to 100 m, and high mean annual ground temperature, between -0.5°C and -1.0°C, at zero annual amplitude depth. Residual thaw layer is occurring annually between the base of the seasonally freezing layer, *ca*. 2 to 3 m, and the top of permafrost at depths, at 4 to 5 m depth. Within the studied area, three shallow boreholes are instrumented, showing ground temperatures from -0.2°C to -0.5°C at 5m depth in two of them, and around +0.8°C in the third. These data evidence highly variable permafrost conditions, with steady and thick permafrost sections at the interfluves and inter-track surfaces, and open and closed taliks under lakes, mires and peatlands, and water tracks.

3. Materials and Methods

Field observations were performed from 5-19 September 2017. Water samples for stable isotope analyses were collected regularly, once in 2-3 days, from the Vorkuta R. and the stream at the water track thalweg, draining into the river near the base camp at the Khanovey station, near its mouth (Figure 1c). Multiple samples were taken along the water track thalweg in its lower reach, downstream from railroad crossing. Several samples were taken from natural hollows, circular depressions *ca.* 0.2…0.4 m in diameter, occurring on the ground surface in the water track valley and on slopes. Several soil pits, 40 to 90 cm deep, were dug at various locations in water track valley and in open tundra to sample shallow subsurface groundwater. Rain water was sampled in Vorkuta, from an intense rain shower occurring on the September 11, 2017. Subpermafrost groundwater was sampled from an artesian well №39-B, near the Khanovey railway station, feeding from a regional aquifer at a depth around 80 m. Water samples were collected in 15 ml conical centrifuge tubes, sealed with Parafilm© and stored at 4°C before they were transported to the lab. All samples (n = 35) were analyzed by multiflow-isotope ratio mass spectrometry at SHIVA platform, EcoLab, Toulouse, France, in December 2017. The internal standard was Vienna Standard Mean Ocean Water (VSMOW).

Dissolved organic carbon (DOC) samples (n = 33) were collected in 20 ml LDPE bottles, pre-washed with weak sulphuric acid and rinsed with MilliQ water. All samples were acidified in the field directly after collection with two drops of 30% H_2SO_4 to suppress biological activity, and stored at 4°C until transported to the lab. The analyses were carried out at VNIRO (All-Russian Research Institute of Fisheries and Oceanography), on a Shimadzu TOC-V analyser.

Electric resistivity tomography (ERT) surveys were performed with 'SKALA-64' ERT station (NEMPHIS, Russia), using a combined three-electrode protocol (AMN-MNB)

Preprints (www.preprints.org) | NOT PEER-REVIEWED | Posted: 21 June 2021 doi:10.20944/preprints202106.0503.v1

with an infinity electrode installed at a distance from 600 to 800 m from the profile. ERT was done at currents between 35 and 70 mA, and survey data were treated with Res2dInv and X2ipi software.

4. Results

4.1. Water stable isotopes

The closest stations of the IAEA Global Network for Isotopes in Precipitation [41] network, providing baseline data for meteoric waters, are located in Pechora and Salekhard, several hundreds of kilometers from the studied location (Table 2). Their data show the effect of different vapour sources and the transformation of isotopic composition of regional precipitation as air masses cross the Polar Ural mountains. At the Pechora site, more than 800 km to the SW from Vorkuta, the local meteoric water line (LMWL) is close to global (GMWL). In Salekhard, *ca.* 300 km to the SE from Vorkuta on the eastern side of the Ural Mountains in the Ob' R. estuary, LMWL plots below the GMWL with an intercept b = 1.83 (±1.79).

Table 2. Isotopic composition of the major water sources in the Bolshaya Zemlya region

Station	Sample source	*n*	Data source	$\delta^{18}O$, ‰SMOW	$\delta^{2}H$, ‰SMOW	d_{ex}, ‰
Pechora	Rain (VIII)		[41]	-12.09±1.76	-80.3±25.0	11.1±8.6
	Rain (IX)		[41]	-12.97±2.10	-87.0±20.0	8.7±3.5
Salekhard	Rain (VIII)		[41]	-13.18±0.68	-100.1±6.0	5.4±3.0
	Rain (IX)		[41]	-13.35±1.71	-102.4±11.1	4.5±4.0
Khanovey	Rain (IX)	1	This work	-14.7	-105	12.3
	Bog	1	" "	-12.72	-92.89	8.9
	Groundwater	1	" "	-15.8	-110	16.1
	Hollows	6	" "	-11.46±0.84	-83.53±3	8.14±4.9
	Lake	1	" "	-10.3	-82.9	-0.7
	River/stream	21	" "	-12.6±0.34	-86.5±3.	14.4±3.3
	Soil pits	4	" "	-13.33±1.40	-94.91±9	11.7±4.4

The local meteoric water line is close to global, and plots slightly above GMWL (Figure 3a), with a LMWL equation:

$$\delta^{2}H = 7.65 \cdot \delta^{18}O + 9.8, \quad (1)$$

The single precipitation event sampled in Vorkuta shows a more depleted isotopic signature compared to long-term September averages for Pechora (Table 2), and relatively high *d*-excess value, evidencing kinetic fractionation and distant moisture sources.

The isotopic composition of rivers and streams (n = 20) departs significantly from the GMWL towards higher d-excess and $\delta^{18}O$ (Table 2 and Figure 3), presumably closer to the mean August rains, in accordance with lower relative humidity of this summer month.

Preprints (www.preprints.org) | NOT PEER-REVIEWED | Posted: 21 June 2021 doi:10.20944/preprints202106.0503.v1

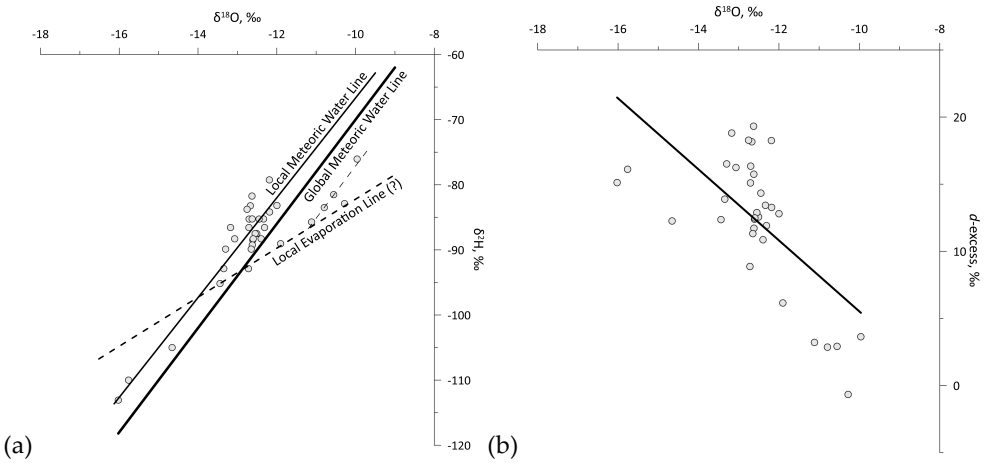

Figure 3. Isotopic composition of water samples, collected in the study area during the field campaign: (a) LMWL in relation to GMWL; (b) $\delta^{18}O$ plotted against *d*-excess.

An evaporation effect is clear in a thermokarst lake sample that has a negative *d*-excess value, and isotopically enriched composition (Table 2), allowing to suggest a local evaporation line slope, as well in several samples from microtopographical hollows, where *d*-excess was low positive and which plot on the mixing line almost in parallel below to the GMWL (Figure 3a).

A single sample of deep subpermafrost groundwater was depleted in ^{18}O, with high d-excess and isotopic signature consistent with that of a confined groundwater, plotting below rainfall and unconfined groundwater sources [42] (Table 2 and Figure 3).

4.2. Dissolved organic carbon

The mean DOC concentration across the dataset is 10.4±5 mg/L; however, it is highly variable for different water bodies (Figure 4). In general, the highest DOC content is observed in standing water, i.e. bogs and hollows, whilst it is significantly lower in streams and rivers.

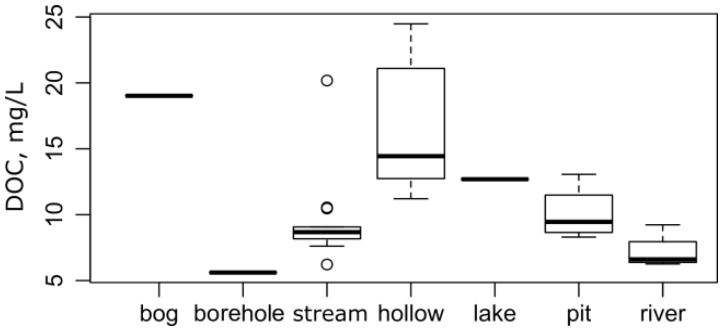

Figure 4. The DOC concentrations across different water bodies in the Khanovey region.

4.3. Electric resistivity tomography (ERT)

The ERT surveys show a highly diverse distribution of high- and low-resistivity grounds in the studied sections (Figure 5), in most cases correlating closely with the hydrographic network features.

Preprints (www.preprints.org) | NOT PEER-REVIEWED | Posted: 21 June 2021 doi:10.20944/preprints202106.0503.v1

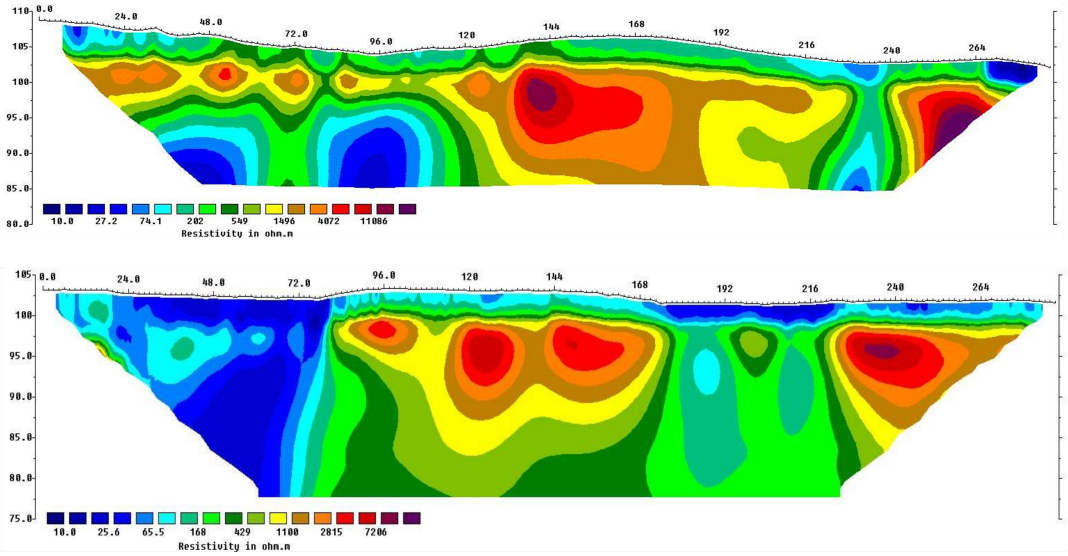

Figure 5. ERT profiles across the transects T1 (top) and T2 (bottom), see Fig. 1c for geographical reference

Geophysical evidence suggests a relatively thick and steady permafrost, exceeding 30 m, persisting under raised non-dissected tundra patches and peat plateaus; a shallow and thin permafrost under a recent mire on the left side of T1 transect (see Figure 5); open taliks under bogs, fens or hummocky depressions. In all cases, the talik walls are sub-vertical, with thaw bulbs slightly expanding downward. This underscores the vulnerability of contemporary permafrost, and also suggests significant groundwater circulation in the talik zones [29].

5. Discussion

5.1. Hydrological connectivity at a catchment scale

The available data on water stable isotopes and their variability, presented in Table 2 and Figure 5, allows a generalized description of hydrological connectivity at a scale of a minor water track catchment. Elevated tundra patches underlain by sandy loams are detached from the hydrological system, and store evaporated water from previous summer months, that was sampled in a soil pit and had $\delta^{18}O$ = -10.55‰, $\delta^{2}H$ = -81.52‰, and d_{ex} = 2.9‰. Other soil pits were opened in water track and drainage network thalwegs and contain water, intermediate between September rainfall and stream/river water, $\delta^{18}O$ = -13.3…-13.4‰, $\delta^{2}H$ = -89.9…-95.2‰, and d_{ex} = 9.9…13.1‰. One pit sample appeared close to the sub-permafrost groundwater, potentially evidencing upward groundwater migration and discharge through the talik zones. This will be discussed in Section 5.4 in more detail.

On the ground surface, multiple hollows were sampled, which were expected to show signis of evaporative loss. Surprisingly, only three out of six sampled hollows were evaporative basins, with mean $\delta^{18}O$ = -10.6±0.6‰ and d_{ex} = 3.23±0.39‰. The other three hollows contained water that was isotopically similar to stream and river water, with $\delta^{18}O$ = -12.4±0.4‰, $\delta^{2}H$ = -87.1±5.1‰, and d_{ex} = 11.7±3‰, assuming their direct connection to shallow sub-surface groundwater and the water track stream. This connection can be assured by the transmissivity feedback effect [43], occurring widely in the organic topsoil outside the elevated tundra patches on better drained soils. Heavily silted and clayey soils, observed locally in the catchment, are saturated and highly thixotropic. At rest, a stiffened thixotropic layer is expected to show barrier functions [44], barring water infiltration, leading to quick saturation of the overlying soil, and initiating rapid water drainage through the organic topsoil.

Preprints (www.preprints.org) | NOT PEER-REVIEWED | Posted: 21 June 2021 doi:10.20944/preprints202106.0503.v1

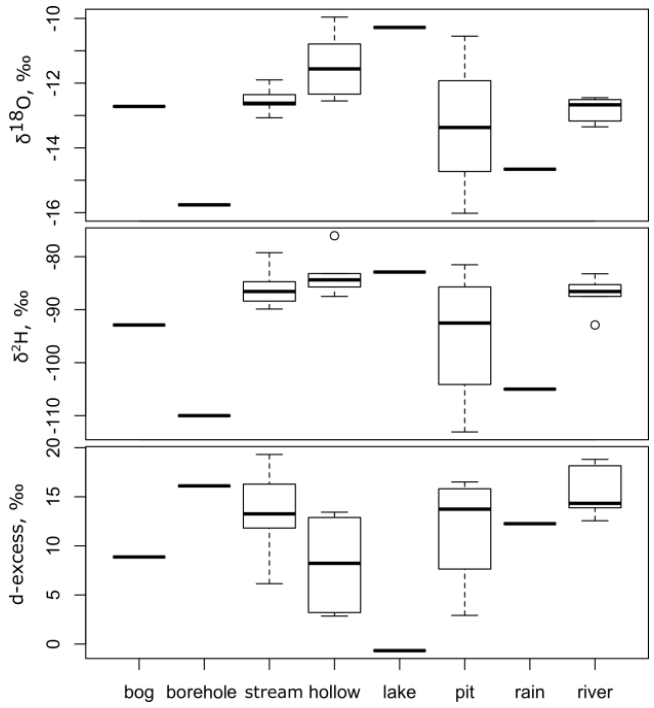

Figure 5. Water stable isotope and d-excess in the water track catchment boxplots, with median, 25% and 75% probability of exceedance shown as bars, highest and lowest as whiskers, and outliers as separate points.

Multiple open-surface bogs in the drainage network depressions exist in the region, and one of them was sampled for water stable isotopes. This water object shows an isotopic signature intermediate between the hollows and the closest stream, which is consistent with the local buffer role of such bogs [45], transforming pluvial runoff, and isotopic signal, and conveying it to streamflow.

5.2 Temporal evolution of water isotopic composition

Paired samples were taken in the Vorkuta R. and at the water track mouth to follow the coevolution of their isotopic composition (Fig. 6). In the major stream, the Vorkuta R., it was gradually shifting toward lighter $\delta^{18}O$ and $\delta^{2}H$ values, reflecting the autumn flow recession and increasing groundwater input, and also potential change in rainwater isotopic signature (Fig. 6a,b). No similar variation in $\delta^{18}O$ values was observed in the water track stream, but at the same time, a progressive depletion in $\delta^{2}H$ was recorded (Fig. 6c).

Deuterium excess values were unexpectedly variable with time in the Vorkuta R., jumping from 12 to 18‰ over the time span of several days (Fig. 6b). Runoff inputs from sources adjacent to the observation point were responsible for the first peak, which coincided with the same *d*-excess peak in the water track stream (Fig. 6d), while more distant sources could potentially contribute to the second peak. The Vorkuta R. has a large basin, around 4000 km^2 at the sampling site, and smoother variations in water chemistry are expected. However, the water isotopic signal of the river could be reset by human activities upstream, *i.e.*, the dam of the Heat Production Station №2 upstream Vorkuta, where the flow is almost ceasing during low-flow periods. In this case, our samples reflect the changes in isotopic composition of major Vorkuta R. tributaries, including Ayach-Yaga R. and Yun'-Yaga R., as well as numerous minor tributaries and water tracks. Low temporal resolution of the survey may add to the lack of smooth variations on the graph.

Preprints (www.preprints.org) | NOT PEER-REVIEWED | Posted: 21 June 2021 doi:10.20944/preprints202106.0503.v1

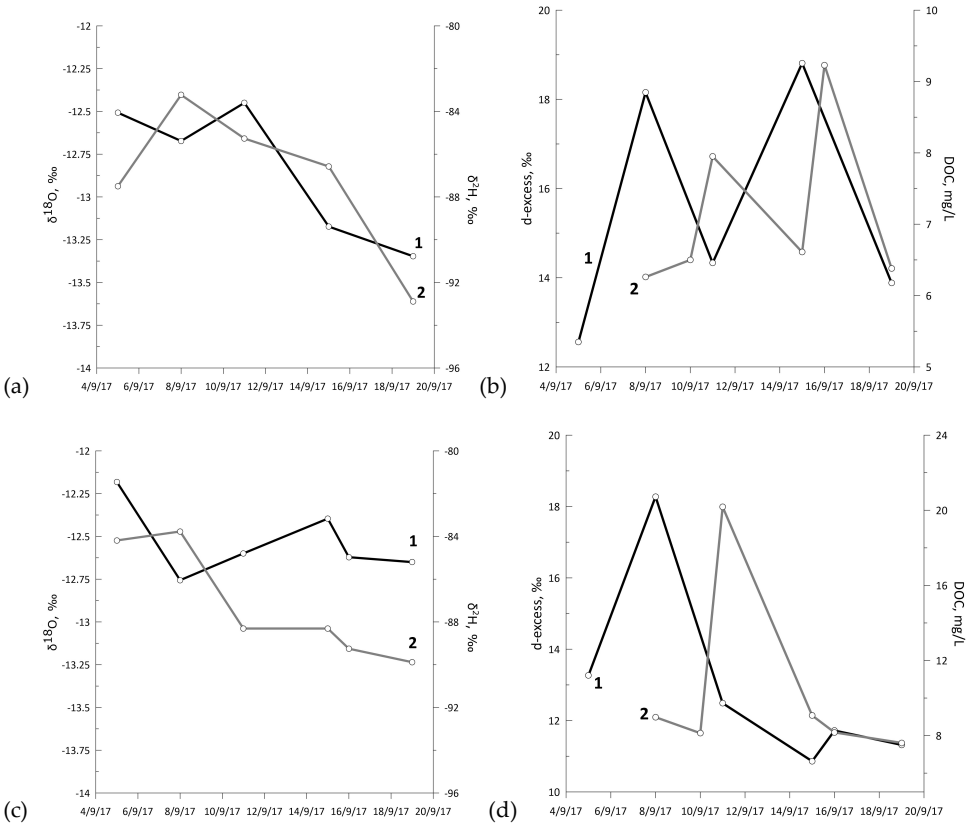

Figure 6. Temporal evolution of isotopic composition (a, c), d-excess and DOC concentrations (b, d) in the Vorkuta R. (a, b) and the water track (c, d). Numbers denote changes in variables shown (1) on the left axis and (2) on the right axis of each graph.

A DOC peaks follows the *d*-excess peak with a three days lag in the water track stream (Fig. 6d). The origin of these peaks is unclear, as is their causal relation. We may hypothesize that the d_{ex} peak at a small catchment scale could have been produced either by preceding rain event, carrying high d_{ex} water, or an increased input from recycled water sources, *e.g.* water condensation from mists on the tundra surface and willow leaves in the water track valley. The DOC peak is then reflecting the slight shift in dominant water sources, from this direct water input, relatively low in DOC, toward bogs/fens and highly-connected zones with shallow subsurface flow.

5.3. DOC export from the catchment

The DOC concentrations are relatively low, and only slightly vary within each water object type (Figure 4). Its highest variability is in pits and hollows, where it follows the variability detected in the isotopic signature. The most evaporated samples, disconnected from subsurface flow, yield also lower DOC values, 11.8±1.7 mg/L on average. In pits and hollows connected to fast subsurface flow, the DOC concentration is 50% higher (17.5±5.3 mg/L), showing an important role they play in the DOC lateral fluxes. Lower DOC content in disconnected hollows may reflect multiple processes, from photodegradation to aerobic microbial degradation, with complex interaction between them [46].

Water track stream discharge is estimated to vary between 2 and 4 L/s, the estimate is based from occasional hydrologic observations from previous years, performed around the same dates in early September and in comparable weather conditions. With average DOC concentration in the water track 9.45 mg/L, and average daily discharge around 3 L/s, daily DOC export for an average day in late autumn equals 2.4 kg/km^2.

 doi:10.20944/preprints202106.0503.v1

5.4. Subpermafrost groundwater input

An 80 m deep artesian well sampled during the course of the study intercepts sub-permafrost groundwater with a distinct isotopic signature (Table 2, Figure 5). Isotopically similar water, highly depleted in ^{18}O ($\delta_{18}O$ = -15.8‰) and with d_{ex} above 15‰, was sampled from a soil pit near the 'Khanovey-2' borehole located in a watertrack thalweg. This soil pit exposed sandy loams down to 0.9m and, when opened, remained almost dry until the water level at the pit slowly settled at a 0.6 m depth. This single sample is not entirely convincing, but combined with geophysical data, it suggests an important connection of shallow subsurface groundwater in water track valleys with deeper waters.

5.5. Water tracks: current and future development

Linear thermokarst features of the Bylot Island, Nunavut, were recently reported to control tundra landscapes by promoting the transition from wet to mesic tundra vegetation in areas adjacent to thermo-erosional gullies [47]. At the study site, and generally in the North-European Arctic Russia, water tracks appear to play the comparable role. Contemporary climate is capable of maintaining wet tundra communities, as evidenced by the abundance of fens in the water track channels on the inferfluves of major rivers of the studied region, at slope summits, shoulders and partially on backslopes. At these positions, slope steepness is insufficient to rapidly convey water downslope even through water tracks. At footslope positions with steeper slopes, water tracks are increasingly efficient to drain the adjacent tundra. Surface subsidence accompanied by permafrost degradation (linear thermokarst) increases the local height difference between the elevated tundra patches and the water track thalwegs, and enhances drainage of these patches. As a result, inter-track elevated tundra hosts mostly xeric communities, with dwarf shrubs and ericaceous species, *i.e.*, red bearberry (*Arctostaphylos rubra*), crowberry (*Empetrum nigrum*), Labrador tea and dwarf birch. Water tracks lower the groundwater table and drain the surrounding tundra effectively enough to maintain xeric habitats.

The water track network in the region is still developing, both vertically and laterally. The studied water track valley (Fig. 2c) is supposedly freshly incised, because its longitudinal profile is non-equilibrium and hosts several major waterfalls, up to *ca.* 1.5 m high. The evolution of the drainage network at the inter-track surface continues. The dominant local slope is directed toward the water track valley, rather than toward the base level of the Vorkuta R. Because of this, we observe the development of new linear depressions on the left side of the water track valley, with depth between 0.15 and 0.30 m, associated with terrain highly disturbed by hummocks.

Climate change is expected to alter the functioning of the water track system of the region but the direction of future change is unclear. Permafrost degradation is expected to promote the gradual lateral thawing of elevated tundra patches now frozen [48]. Visual inspection of satellite imagery shows that there is significant difference between water track network on south- and north-facing slopes, hence increasing insolation and air temperature in the future climate are expected to produce significant geomorphic response.

6. Conclusions

The hydrological snapshot of a small tundra catchment in the north-European Russia provides several insights into the hydrological connectivity within its limits. Elevated tundra patches appear to be disconnected from the stream, while the slopes and the riparian zone contribute actively, though locally, to the stream runoff. Minor hollows are found to be either connected to the shallow subsurface runoff, or disconnected from it. The difference in connectivity is traceable via *d*-excess; the disconnected hollows act as evaporative basins and have lower *d*-excess values. The connected hollows also serve as

important DOC flux conveyors, with DOC concentrations up to 50% higher than in disconnected hollows.

Author Contributions: Conceptualization and methodology, N.T.; field investigation, N.T., V.I., D.S., P.K. and O.K.; writing – original draft preparation, N.T.; writing – review and editing, N.T., D.S., and P.K.; visualization, N.T. and O.K. All authors have read and agreed to the published version of the manuscript.

Funding: This study was conducted with support from RuNoCore: Russian-Norwegian research-based education in cold regions engineering (#CPRU-2017/10015), funded by Norwegian Center for International Cooperation in Education (SIU). The manuscript was prepared under the implementation of the state task and the research plan of the IEG RAS, Research Topic AAAA-A19-119021190077-6, and Melnikov Permafrost Institute SB RAS, Research Topic AAAA-A20-120111690008-9.

Data Availability Statement: The analyzed dataset is available through Figshare, an open repository, and accessible by DOI: 10.6084/m9.figshare.14502003.

Acknowledgments: The authors acknowledge the support from the Northern Railroad services in arranging the field surveys.

Conflicts of Interest: The authors declare no conflict of interest. The funders had no role in the design of the study; in the collection, analyses, or interpretation of data; in the writing of the manuscript, or in the decision to publish the results.

References

1. Bracken, L.J.; Croke, J. The concept of hydrological connectivity and its contribution to understanding runoff-dominated geomorphic systems. *Hydrol Process* **2007**, *21*, 1749–1763. DOI: 10.1002/hyp.6313.
2. Cammeraat, L.H. A review of two strongly contrasting geomorphological systems within the context of scale. *Earth Surf Process Landforms* **2002**, *27*, 1201–1222. DOI: 10.1002/esp.421.
3. Pringle, C. What is hydrologic connectivity and why is it ecologically important? *Hydrol Process* **2003**, *17*, 2685-2689. DOI: 10.1002/hyp.5145.
4. Bracken, L.J.; Wainwright, J.; Ali, G.A.; Tetzlaff, D.; Smith, M.W.; Reaney, S.M.; Roy, A.G. Concepts of hydrological connectivity: Research approaches, pathways and future agendas. *Earth Sci. Rev.* **2013**, *119*, 17-34. DOI: 10.1016/j.earscirev.2013.02.001.
5. Guzmán, P.; Anibas, C.; Batelaan, O. ; Huysmans, M.; Wyseure, G. Hydrological connectivity of alluvial Andean valleys: a groundwater/surface-water interaction case study in Ecuador. *Hydrogeol J* **2016**, *24*, 955–969. DOI: 10.1007/s10040-015-1361-z.
6. Woo, M.-K. *Permafrost Hydrology*. Springer Verlag, 2012, 575 pp.
7. Tananaev, N.; Teisserenc, R.; Debolsky, M. Permafrost hydrology research domain: process-based adjustment. *Hydrology* **7**, *6*. DOI: 10.3390/hydrology7010006.
8. Gao, H.; Wang, J.; Yang, Y.; Pan, X.; Ding, Y.; Duan, Z. Permafrost hydrology of the Qinghai-Tibet Plateau: A review of processes and modeling. *Front Earth Sci* **2021**, *8*, 576838. DOI: 10.3389/feart.2020.576838.
9. Boike, J.; Roth, K.; Overduin, P.P. Thermal and hydrologic dynamics of the active layer at a continuous permafrost site (Taymyr Peninsula, Siberia). *Wat Resourc Res* **1998**, *34*, 355–363.
10. Shepelev, V.V. Suprapermafrost waters of the cryolithosphere and their classification. *Geogr Nat. Resourc* **2009**, *30(2)*, 151-155. DOI: 10.1016/j.gnr.2009.06.011.
11. Fotiev, S.M. Underground waters of cryogenic areas of Russia. Earth's Cryosphere **2013**, *XVII (2)*, 41-59 (in Russian).
12. Gooseff, M.N.; Wlostowski, A.; McKnight, D.M.; Jaros, C. Hydrologic connectivity and implications for ecosystem processes - Lessons from naked watersheds. *Geomorphology* **2017**, *277*, 63-71. DOI: 10.1016/j.geomorph.2016.04.024.
13. Briggs, M.A.; Walvoord, M.A.; McKenzie, J.M.; Voss, C.I.; Day-Lewis, F.D.; Lane, J.W. New permafrost is forming around shrinking Arctic lakes, but will it last? *Geophys Res Lett* **2014**, *41*, 1585–1592. DOI: 10.1002/2014GL059251.
14. Ling, F.; Wu, Q.; Zhang, T.; Niu, F. Modelling open-talik formation and permafrost lateral thaw under a thermokarst lake, Beiluhe basin, Qinghai-Tibet Plateau. *Permafr Periglac Process* **2012**, *23*, 312-321. DOI: 10.1002/ppp.1754.
15. You, Y.; Yu, Q.; Pan, X.; Wang, X.; Guo, L. Geophysical imaging of permafrost and talik configuration beneath a thermokarst lake. *Permafr Periglac Process*, **17**, *28*, 470–476. DOI: 10.1002/ppp.1938.
16. Pavlova, N.; Lebedeva, L.; Efremov, V. Lake water and talik groundwater interaction in continuous permafrost, Central Yakutia. *E3S Web Conf* **2019**, *98*, 07024. DOI: 10.1051/e3sconf/20199807024.
17. Wellman, T.P.; Voss, C.I.; Walvoord, M.A. Impacts of climate, lake size, and supra- and sub-permafrost groundwater flow on lake-talik evolution, Yukon Flats, Alaska (USA). *Hydrogeol J* **2013**, *21*, 281–298. DOI: 10.1007/s10040-012-0941-4.
18. Connon, R.F.; Quinton, W.L.; Craig, J.R.; Hayashi, M. Changing hydrologic connectivity due to permafrost thaw in the lower Liard River valley, NWT, Canada. *Hydrol Process* **2014**, *28*, 4163–4178. DOI: 10.1002/hyp.10206.
19. Walvoord, M.A.; Kurylyk, B.L. Hydrologic impacts of thawing permafrost – A review. *Vadoze Zone J* **2016**, *15*, 1–20. DOI: 10.2136/vzj2016.01.0010.

20. Lamontagne-Hallé, P.; McKenzie, J.M.; Kurylyk, B.L.; Zipper, S.C. Changing groundwater discharge dynamics in permafrost regions. *Environ Res Lett* **2018**, *13*, 084017. DOI: 10.1088/1748-9326/aad404.
21. Hayashi, M; Quinton, W.L.; Pietroniro, A.; Gibson, J.J. Hydrologic functions of wetlands in a discontinuous permafrost basin indicated by isotopic and chemical signatures. *J Hydrol* **2004**, *296*, 81–97. DOI: 10.1016/j.jhydrol.2004.03.020.
22. Tetzlaff, D.; Piovano, T.; Ala-Aho, P.; Smith, A.; Carey, S.K.; Marsh, P.; Wookey, P.A.; Street, L.E.; Soulsby, C. Using stable isotopes to estimate travel times in a data-sparse Arctic catchment: Challenges and possible solutions. *Hydrol Process* **2018**, *32*, 1936–1952. DOI: 10.1002/hyp.13146.
23. Throckmorton, H.M.; Newman, B.D.; Heikoop, J.M.; Perkins, G.B.; Feng, X.; Graham, D.E.; O'Malley, D.; Vesselinov, V.V.; Young, J.; Wullschleger, S.D.; Wilson, C.J. Active layer hydrology in an arctic tundra ecosystem: quantifying water sources and cycling using water stable isotopes. *Hydrol Process* **2016**, *30*, 4972–4986. DOI: 10.1002/hyp.10883.
24. Wan, C.; Gibson, J.J.; Peters, D.L. Isotopic constraints on water balance of tundra lakes and watersheds affected by permafrost degradation, Mackenzie Delta region, Northwest Territories, Canada. *Sci Tot Env* **2020**, *731*, 139176. DOI: 10.1016/j.scitotenv.2020.139176.
25. Brooks, J.R.; Mushet, D.M.; Vanderhoof, M.K.; Leibowitz, S.G.; Christensen, J.R.; Neff, B.P.; Rosenberry, D.O.; Rugh, W.D.; Alexander, L.C. Estimating wetland connectivity to streams in the prairie pothole region: an isotopic and remote sensing approach. *Water Resourc Res* **2018**, *54*, 955–977. DOI: 10.1002/2017WR021016.
26. Gibson, J.J.; Yi, Y.; Birks, S.J. Isotopic tracing of hydrologic drivers including permafrost thaw status for lakes across Northeastern Alberta, Canada: A 16-year, 50- lake assessment. *J Hydrol Region Stud* **2019**, *26*, 100643. DOI: 10.1016/j.ejrh.2019.100643.
27. Welp, L.R.; Randerson, J.T.; Finlay, J.C.; Davydov, S.P.; Zimova, G.M.; Davydova, A.I.; Zimov, S.A. A high-resolution time series of oxygen isotopes from the Kolyma River: Implications for the seasonal dynamics of discharge and basin-scale water use. *Geophys Res Lett* **2005**, *32*, L14401. DOI: 10.1029/2005GL022857.
28. Gibson, J.J.; Birks, S.J.; Yi, Y. Stable isotope mass balance of lakes: a contemporary perspective. *Quatern Sci Rev* **2016**, *131*, 316–328. DOI: 10.1016/j.quascirev.2015.04.013.
29. Devoie, E.G.; Craig, G.R.; Connor, R.F.; Quinton, W.L. Taliks: A tipping point in discontinuous permafrost degradation in peatlands. *Water Resourc Res* **2019**, *55*, 9838–9857. DOI: 10.1029/2018WR024488.
30. Marchenko, S.S.; Gorbunov, A.P.; Romanovsky, V.E. Permafrost warming in the Tien Shan Mountains, Central Asia. *Glob Planet Change* **2007**, *56*, 311–327. DOI: 10.1016/j.gloplacha.2006.07.023.
31. Streletsky, D.A.; Tananaev, N.I.; Opel, T.; Shiklomanov, N.I.; Nyland, K.; Streletskaya, I.D.; Tokarev, I.; Shiklomanov, A.I. Permafrost hydrology in changing climatic conditions: seasonal variability of stable isotope composition in rivers in discontinuous permafrost. *Environ Res Lett* **2015**, *10*, 095003. DOI: 10.1088/1748-9326/10/9/095003.
32. Ala-aho P.; Soulsby, C.; Pokrovsky, O.S.; Kirpotin, S.N.; Karlsson, J.; Serikova, S.; Vorobyev, S.N.; Manasypov, R.M.; Loiko, S.; Tetzlaff, D. Using stable isotopes to assess surface water source dynamics and hydrological connectivity in a high-latitude wetland and permafrost influenced landscape. *J Hydrol* **2018**, *556*, 279–293. DOI: 10.1016/j.jhydrol.2017.11.024.
33. Roy-Leveillee, P.; Burn, C.R. Near-shore talik development beneath shallow water in expanding thermokarst lakes, Old Crow Flats, Yukon. *J Geophys Res Earth Surf.* **2017**, *122*, 1070–1089. DOI: 10.1002/2016JF004022.
34. Disher, B.S.; Connon, R.F.; Haynes, K.M.; Hopkinson, C.; Quinton, W.L. The hydrology of treed wetlands in thawing discontinuous permafrost regions. *Ecohydrol* **2021**. DOI: 10.1002/eco.2296.
35. Sjöberg, Y.; Marklund, P.; Pettersson, R.; Lyon, S.W. Geophysical mapping of palsa peatland permafrost. *The Cryosphere* **2015**, *9*, 465–478. DOI: 10.5194/tc-9-465-2015.
36. Evans, S.G.; Ge, S. Contrasting hydrogeologic responses to warming in permafrost and seasonally frozen ground hillslopes. *Geophys Res Lett* **2017**, *44*, 1803–1813. DOI: 10.1002/2016GL072009.
37. Walvoord, M.A.; Striegl, R.G. Increased groundwater to stream discharge from permafrost thawing in the Yukon River basin: Potential impacts on lateral export of carbon and nitrogen. *Geophys Res Lett* **2007**, *34*, L12402. DOI: 10.1029/2007GL030216.
38. Goudie, A.S. Global warming and fluvial geomorphology. Geomorphology **2006**, *79*, 384-394. DOI: 10.1016/j.geomorph.2006.06.023.
39. Isaev, V.; Kotov, P.; Sergeev, D. Technogenic hazards of Russian North Railway. In *Transportation Soil Engineering in Cold Regions*. *Lecture Notes in Civil Engineering. Vol. 49*; Petriaev, A., Konon, A., Eds.; Publisher: Springer, Singapore, 2020; Volume 1, pp. 311–320. DOI: 10.1007/978-981-15-0450-1_32.
40. Trochim, E.D.; Jorgenson, M.T.; Prakash, A.; Kane, D.L. Geomorphic and biophysical factors affecting water tracks in northern Alaska. *Earth Space Sci* **2016**, *3*, 123–141. DOI: 10.1002/2015EA000111.
41. International Atomic Energy Agency/World Meteorological Organization (IAEA/WMO). Global Network of Isotopes in Precipitation (GNIP). https://nucleus.iaea.org/Pages/GNIPR.aspx (accessed: 18.04.2021).
42. De Wet, R.F.; West, A.G.; Harris, C. Seasonal variation in tap water δ^2H and $\delta^{18}O$ isotopes reveals two tap water worlds. *Sci Rep* **2020**, *10*, 13544. DOI: 10.1038/s41598-020-70317-2.
43. Kendall, K.A.; Shanley, J.B.; McDonnell, J.J. A hydrometric and geochemical approach to test the transmissivity feedback hypothesis during snowmelt. *J Hydrol* **1999**, *219*, 188-205. DOI: 10.1016/S0022-1694(99)00059-1.
44. Ren, Y.; Yang, S.; Andersen, K.H.; Yang, Q.; Wang, Y. Thixotropy of soft clay: A review. *Eng Geol* **2021**, *287*, 106097. DOI: 10.1016/j.enggeo.2021.106097.
45. Veizaga, E.A.; Ocampo, C.J.; Rodríguez, L. Hydrological and hydrochemical behavior of a riparian zone in a high-order flatland stream. *Environ Monit Assess* **2019**, *191*, 10. DOI: 10.1007/s10661-018-7136-y.

46. Cory, R.M.; Kling, G.W. Interactions between sunlight and microorganisms influence dissolved organic matter degradation along the aquatic continuum. *Limnol Oceanogr Lett* **2018**, *3*, 102–116. DOI: 10.1002/lol2.10060.
47. Perreault, N.; Lévesque, E.; Fortier, D.; Lamarque, L.J. Thermo-erosion gullies boost the transition from wet to mesic tundra vegetation. *Biogeosci* **2016**, *13*, 1237–1253. DOI: 10.5194/bg-13-1237-2016.
48. Douglas, T.A.; Hiemstra, C.A.; Anderson, J.E.; Barbato, R.A.; Bjella, K.L.; Deeb, E.J.; Gelvin, A.B.; Nelsen, P.E.; Newman, S.D.; Saari, S.P.; Wagner, A.M. Recent degradation of Interior Alaska permafrost mapped with ground surveys, geophysics, deep drilling, and repeat airborne LiDAR. *The Cryosphere Discuss* **2021**. DOI: 10.5194/tc-2021-47.